Am J Physiol Heart Circ Physiol 310: H572–H586, 2016.
First published December 23, 2015; doi:10.1152/ajpheart.00773.2015.

Dissecting the role of the myofilament in diaphragm dysfunction during the development of heart failure in mice

Todd E. Gillis,[1,2] Jordan M. Klaiman,[1,2] Andrew Foster,[2,3] Mathew J. Platt,[2,3] Jason S. Huber,[2,3] Melissa Y. Corso,[2,3] and Jeremy A. Simpson[2,3]

[1]*Department of Integrative Biology, University of Guelph, Guelph, Ontario, Canada;* [2]*Cardiovascular Research Center, University of Guelph, Guelph, Ontario, Canada; and* [3]*Department of Human Health and Nutritional Sciences, University of Guelph, Guelph, Ontario, Canada*

Submitted 7 October 2015; accepted in final form 21 December 2015

Gillis TE, Klaiman JM, Foster A, Platt MJ, Huber JS, Corso MY, Simpson JA. Dissecting the role of the myofilament in diaphragm dysfunction during the development of heart failure in mice. *Am J Physiol Heart Circ Physiol* 310: H572–H586, 2016. First published December 23, 2015; doi:10.1152/ajpheart.00773.2015.—Dyspnea and reduced exercise capacity, caused, in part, by respiratory muscle dysfunction, are common symptoms in patients with heart failure (HF). However, the etiology of diaphragmatic dysfunction has not been identified. To investigate the effects of HF on diaphragmatic function, models of HF were surgically induced in CD-1 mice by transverse aortic constriction (TAC) and acute myocardial infarction (AMI), respectively. Assessment of myocardial function, isolated diaphragmatic strip function, myofilament force-pCa relationship, and phosphorylation status of myofilament proteins was performed at either 2 or 18 wk postsurgery. Echocardiography and invasive hemodynamics revealed development of HF by 18 wk postsurgery in both models. In vitro diaphragmatic force production was preserved in all groups while morphometric analysis revealed diaphragmatic atrophy and fibrosis in 18 wk TAC and AMI groups. Isometric force-pCa measurements of myofilament preparations revealed reduced Ca^{2+} sensitivity of force generation and force generation at half-maximum and maximum Ca^{2+} activation in 18 wk TAC. The rate of force redevelopment (k_{tr}) was reduced in all HF groups at high levels of Ca^{2+} activation. Finally, there were significant changes in the myofilament phosphorylation status of the 18 wk TAC group. This includes a decrease in the phosphorylation of troponin T, desmin, myosin light chain (MLC) 1, and MLC 2 as well as a shift in myosin isoforms. These results indicate that there are multiple changes in diaphragmatic myofilament function, which are specific to the type and stage of HF and occur before overt impairment of in vitro force production.

calcium-activated force generation; diaphragm function; heart failure; myofilament proteins; protein phosphorylation

NEW & NOTEWORTHY

Diaphragmatic myofilament function becomes increasingly impaired during the development of early heart failure, caused by transverse aortic constriction, and these changes occur in parallel with a decrease in the phosphorylation of key regulatory proteins. This loss of myofilament function and alterations to the contractile proteins precede impairment of the intact diaphragm.

HEART FAILURE (HF) is a global health problem and is one of the most prevalent causes of morbidity in all ages (15, 46). Patients with HF are frequently limited in their daily activities by dyspnea and exertional fatigue. One potential cause is inspiratory muscle (primarily the diaphragm) dysfunction. De Troyer and colleagues (11) first noted compromised inspiratory muscle function in patients with cardiac dysfunction. Respiratory muscle dysfunction is now considered a salient feature of patients (11, 21, 23, 35, 36, 62) and animals (7–9, 24, 28, 53, 58) with HF. Currently, little is known about the development of respiratory muscle dysfunction during the early onset of HF.

In patients with HF, eupneic pressure generation is increased (28, 58), which is considered to impose a stress on the diaphragm. This chronic workload on the diaphragm is thought to overwork the muscle leading to development of a myopathy characterized by a shift in fiber type, atrophy, and contractile dysfunction. With the development of HF, there is an increase in the relative proportion of type I (slow oxidative twitch) fibers in the diaphragm (8, 9, 63, 64). In contrast, limb muscles show an increase in the proportion of type IIb (fast glycolytic twitch) fibers (12, 31, 34, 55, 56), which is attributed, in part, to deconditioning. Thus a shift from fast- to slow-twitch muscle fibers would imply fatigue resistance at the cost of reduced maximal force-generating capacity of the diaphragm with the opposite occurring in the peripheral limb muscles. However, the decrease in maximal inspiratory pressure generation cannot solely be accounted for by a change in the proportion of slow-twitch fibers. Indeed, histological evaluation of the diaphragm from HF shows extensive atrophy (24, 53), fibrosis, and other abnormalities (30).

Diaphragm dysfunction has been investigated using a variety of animal models where HF was induced by genetic (i.e., dilated and hypertrophic cardiomyopathies) and surgical manipulations (ligation of the left anterior descending artery to induce a MI or constriction of the aorta to cause, a volume and pressure overload, respectively) in various species (e.g., rabbits, rats, hamsters and mice). In all studies, although diaphragm function was impaired, the methods used to characterize function varied, making cross-study interpretations difficult. The underlying assumption is that diaphragm dysfunction is a common feature of heart failure and independent of the type and stage of heart failure. Further, there has been little study of diaphragm function in the early stages of heart failure as previous work has targeted late or end-stage HF. By understanding the incipient events leading to the development of diaphragm dysfunction, only then can future studies begin to investigate treatment options that have a realistic goal of leading to new clinical treatment strategies. Therefore, it is neither clear if different perturbations of HF cause similar functional responses in the diaphragm nor if diaphragmatic dysfunction occurs early in the progression of the disease.

Address for reprint requests and other correspondence: T. E. Gillis, Dept. of Integrative Biology, Univ. of Guelph, Guelph, ON, N1G-2W1 Canada (e-mail: tgillis@uoguelph.ca).

One factor that determines the active properties of striated muscle is the sensitivity of the contractile element to Ca^{2+}. Muscle contraction is triggered when Ca^{2+} binds to the actin thin-filament, via the troponin (Tn) complex. The end result is an increased mobility of tropomyosin (Tm) over the surface of the actin filaments, allowing for the formation of force-generating cross-bridges between actin and myosin (13, 19). Manipulation of the Ca^{2+} sensitivity of the contractile element can affect the amount of force generated as well as the rate at which it is generated (17, 19). Such changes in contractile function can be caused by alterations to the proteins that compose the contractile element (17, 22, 67). The loss of diaphragm function during the development of HF may therefore be due, in part, to changes to the contractile elements of the muscle fibers composing the diaphragm. Previous work has demonstrated that the diaphragm of rats in end-stage heart failure can contain less myosin (66) and increased levels of myosin heavy chain oxidation (8). These studies indicate that the myofilament is playing a role in diaphragm dysfunction during heart failure. However, there has been no study to date that has effectively examined how other components of the diaphragm myofilament are affected during the development of heart failure and how this may translate to a loss of contractility.

In the current study, we examined how the development of HF in mice, caused by a pressure overload, influenced the contractile function of diaphragm muscle after 2 and 18 wk of transverse aortic constriction (TAC). We further compared the observed diaphragm dysfunction in pressure-overload HF to those in HF at 18 wk following a myocardial infarction (MI). Diaphragm contractility was characterized by measuring the Ca^{2+} activation of force generation by chemically skinned preparations composed of multiple fibers. We also examined the isoforms of myosin heavy chain (MyHC) in the muscle as well as the phosphorylation status of the myofilament proteins. The results demonstrate that the contractile function of the diaphragm myofilament becomes increasingly compromised following the induction of a pressure overload; this loss of diaphragm function is more significant than in response to a myocardial infarction.

METHODS

In vivo hemodynamics and cardiac morphometrics. All experimental procedures were approved by the institutional animal care committee and conducted in accordance with the guidelines of the Canadian Council on Animal Care as set out in the Guide to the Care and Use of Experimental Animals. All experiments were conducted on male CD-1 mice (Charles River, Laval QC) housed in a 12:12-h light-dark facility with food and water ad libitum.

Pressure-overload HF induced by transverse aortic constriction (TAC). Transverse aortic constriction was performed as previously described (4). In brief, 9-wk-old mice (~35 g body wt) were anesthetized with a minimum alveolar concentration (MAC) of 5% isoflurane in 100% O_2 and were maintained in the surgical plane of anesthesia with a MAC of 2% isoflurane in 100% O_2. Mice were then orotracheally intubated using a 20 gauge angiocatheter (Becton-Dickinson, Franklin Lakes, NJ) and mechanically ventilated with a rodent microvent (Harvard Apparatus, Saint-Laurent, QC) at an approximate tidal volume of 200 μl and 150 breaths/min. Ribs were separated from the sternum at their cartilaginous insertions and the transverse aorta was isolated; 7-0 silk thread was tied around the transverse aorta between the brachiocephalic artery and left common carotid artery to the diameter of a 26-gauge needle. After removing the needle, 5-0 Sofsilk sutures were used to suture the ribs and skin. Animals were administered analgesic at need and were carefully monitored for postsurgical complications. Those that displayed abnormalities or complications were removed from the experimental group whereas those that were included in the study progressed to 2 or 18 wk of TAC.

HF caused by myocardial infarction (MI) via ligation of the left anterior descending coronary artery. Nine-week-old mice (~35 g body wt) were anesthetized and prepared for surgery as described above. MI was induced by with surgipro II polypropylene suture (Covidien, Saint-Laurent, QC) just inferior to the atrioventricular boarder. Silk 5-0 Sofsilk sutures were used to suture both the ribs and the skin. Animals were administered analgesic as required and were carefully monitored for postsurgical complications. Those that displayed abnormalities or complications were removed from the experimental group whereas those that were included in the study progressed to 18 wk post MI.

Echocardiographic and hemodynamic analysis. For echocardiography and cardiac catheterization, mice were anesthetized with a MAC of 2% isoflurane in 100% and body temperature was maintained at 37°C. Transthoracic 2D and M-mode echocardiography were performed from the long-axis view of the heart at the level of the papillary muscle with a Visualsonics Vevo 2100 imaging system (Visualsonics, Toronto, ON) equipped with a 40-MHz linear transducer (MS550D). Measurements were averaged from five separate cardiac cycles.

For invasive hemodynamic analysis, a 1.2-Fr catheter (FTS-1211B-0018; Scisense, London, ON) was inserted into the right carotid and advanced retrograde into the LV; hemodynamic signals were digitized at a sampling rate of 2 kHz and recorded using iWorx analytic software (Labscribe2, Dover, NH). Following data collection, tissues were weighed and either frozen in liquid nitrogen for protein biochemistry, harvested for isolated diaphragm strip, myofilament force-pCa analysis, or fixed for histology.

Histology. All samples were fixed in 10% buffered formalin, processed, and embedded in paraffin. Cross sections of the diaphragm and heart were stained with Picosirius Red to quantify fibrosis and measure cross-sectional area (CSA). Images were acquired using an Olympus FSX 100 light microscope and analyzed using Cell Sense software (Olympus, Tokyo, Japan).

In vitro diaphragm contractility. Diaphragm muscle was quickly excised and placed in Krebs-Henseleit solution (mM/l: 118 NaCl, 4.7 KCl, 1.2 KH_2PO_4, 1.2 $MgSO_4 \cdot 7\ H_2O$, 27.26 $NaHCO_3$, 11.1 glucose, 2.3 $CaCl_2 \cdot 2H_2O$, 10 units/l insulin and 3.0×10^{-4} g/l curare) at room temperature and pH 7.4. A triangular section of diaphragm was removed with central tendon and rib intact; 5-0 silk ties were secured to the central tendon and ribs, which were respectively attached to a force transducer (Grass instruments, Warwick, RI) and stationary hook. Stimulating electrodes were placed on both sides of the diaphragm section; tissue was immersed in Krebs-Henseleit bicarbonate buffer that was warmed to 27°C and aerated with 95% O_2-5% CO_2 (pH of 7.4). Diaphragm strips were elongated to their optimal length (*Lo*: muscle length which produced maximal force at 100-Hz stimulation) via a micromanipulator attached to the force transducer. After a 45-min thermoequilibration period, peak force production was determined. Isometric contractility data were collected on AcqKnowledge software (BIOPAC systems, Goleta, CA) and analyzed using Spike2 software (Cambridge Electronic Design, Cambridge, UK). Force production was normalized to physiological cross-sectional area assuming a muscle density of 1.06 g/ml; optimal muscle length was not different between any of the groups and ranged between 1.0 and 1.1 cm.

Ca^{2+} activation of skinned diaphragm preparations. Mechanical experiments were conducted on permeabilized preparations dissected from the diaphragm of the sham (control) and surgically treated mice. Following removal from the thoracic cavity, each diaphragm was immediately placed in ice-cold physiological saline (in mM: 94 NaCl,

24 $NaCO_3$, 5 KCl, 1 $MgSO_4$, 1 Na_2HPO_4, 0.7 $CaCl_2$, pH 7.6 at 15°C). Blood was washed from the diaphragm before it was pinned out on a chilled dissection stage (Fig. 1*A*) containing ice-cold relaxing solution (in mM: 100 KCl, 10 MOPS, 5 dipotassium EGTA, 9 $MgCl_2$, 4 NaATP, 20 2–3-butanedione monoxime pH 7.0 at 4°C) (18). Butanedione monoxime (BDM) inhibits cross-bridge formation and was used to reduce contracture-induced injury. Protease inhibitors [i.e., phenylmethanesulfonylfluoride (PMSF), leupeptin and benzamidine] were in all relaxing and skinning solutions. The relaxing solution was replaced with ice-cold skinning solution containing glycerol (50% vol:vol) and Triton X-100 (1%). The diaphragms were skinned overnight at 4°C with one solution change as demonstrated previously (18). The following morning, the skinning solution was replaced with the same solution without Triton X-100; diaphragm preparations were then stored at −20°C until utilized (maximum 2 days). The experimental preparations were dissected from the skinned diaphragm on a chilled microscope stage using a razor blade fragment held by a clamp. Muscle strips were dissected randomly from throughout the diaphragm to ensure the functional data were representative of the entire multifiber type tissue. Each strip was then visualized under polarized light to determine if the fibers were in parallel. The ends of the preparations were chemically fixed using 1% glutaraldehyde, and then wrapped in aluminum foil T-clips (Kem-mil, CA). These T-clips were 1.0 mm in length and 1.2 mm in width with a small hole in one end to allow the preparation to be mounted to the experimental apparatus via steel hooks (Fig. 1*B*).

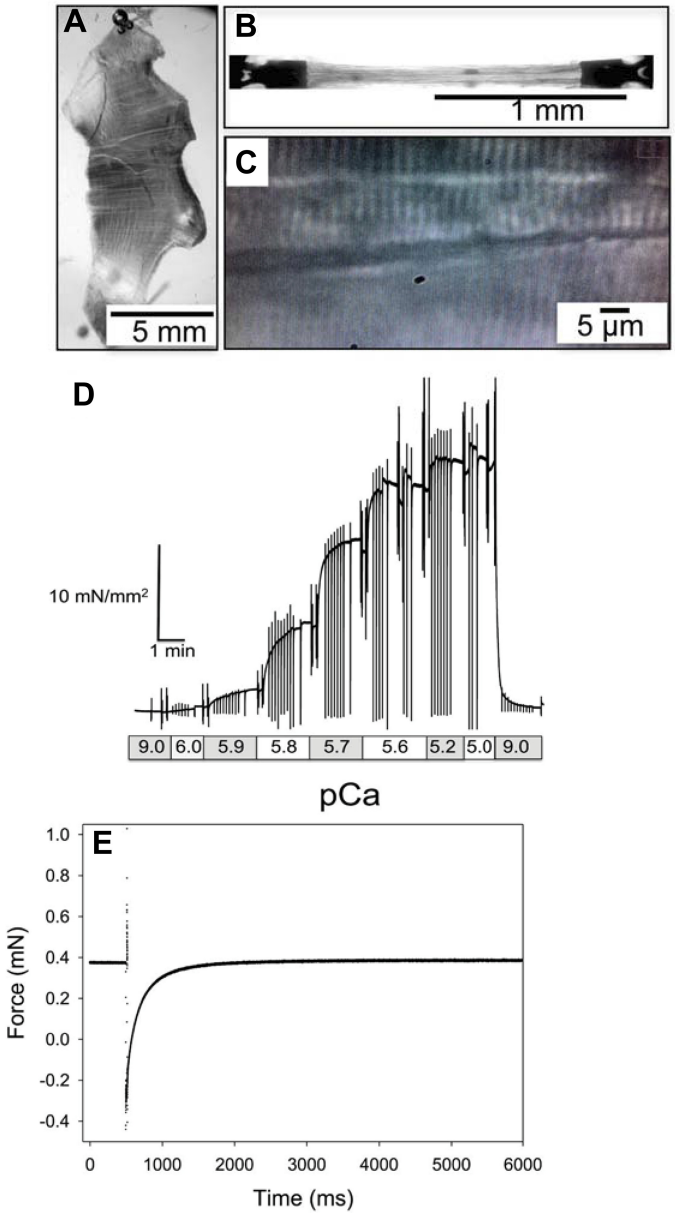

Fig. 1. Details of experimental preparation and representative force and rate measurements. *A*: single lobe of skinned mouse diaphragm. *B*: diaphragm preparation with ends wrapped in aluminum t-clips. *C*: sarcomere pattern of preparation at 400X magnification. *D*: sample force trace resulting from the Ca^{2+} activation of a muscle preparation from a sham mouse. *E*: force output during k_{tr} measurement following rapid release-restretch of a diaphragm preparation from a sham mouse at pCa 5.0. Force was normalized relative to maximal force generated (F_{max}); pCa values are indicated along the bottom of the trace in *D*. The noise on the force trace is motor movements (during k_{tr} measurements or the Brenner cycling used to maintain myofilament integrity). k_{tr} is used as a measure of the rate of cross-bridge cycling during Ca^{2+} activation.

Muscle mechanics instrument. The mechanical measurements were made using a custom instrument from Aurora Scientific (Aurora, ON) mounted on the stage of an inverted microscope (Model Eclipse TE 2000U, Nikon Japan). The instrument, as previously described, is composed of a permeabilized fiber test system (model 802B, Aurora Scientific), a force transducer (model 400A, 2.0-kHz resonant frequency, Aurora Scientific) and a servo-motor (model 308C, Aurora Scientific) tuned for a 250-μs step response (16). Temperature was maintained within 1°C of set temperature. Sarcomere length (SL) was measured by fast Fourier transform (FFT) analysis using a high-speed video sarcomere length system (model 901A, Aurora Scientific) with a CCD camera (model VGA-210-LMCN, Imperx, FL) with 640 × 480 resolution. The camera images the preparation through a 40× objective with a 3-mm working distance (Nikon, Mississauga, ON) (Fig. 1*C*).

Solutions for mechanical measurements. Solution composition was determined according to an iterative computer program that calculates the equilibrium concentration of ligands and ions based on published affinity constants. Activation solutions contained (in mM): 15 phosphocreatine, 15 EGTA, at least 40 3-(*N*-morpholino)propanesulfonic acid (MOPS), 1 free Mg^{2+}, 135 $Na^+ + K^+$, 1 dithiothreitol (DTT), 250 units/ml creatine phosphokinase (CPK) (Sigma, St. Louis, MO), and 5 NaATP, pH 7.0 at 15°C. Ionic strength was 0.17 M. The Ca^{2+} level (expressed as $pCa = -\log[Ca^{2+}]$) was varied between pCa 9.0 and pCa 5.0 by adjusting $CaCl_2$ as in Gillis et al. (18).

Mechanical measurements. The Ca^{2+} activation of the diaphragm preparations was characterized using methods previously described (16, 18). Briefly, the preparation was mounted onto the apparatus by attaching the T-clips on the muscle to steel hooks attached to the force transducer and servomotor. Sarcomere length was measured by analyzing the sarcomere pattern at multiple locations (>10) throughout the preparation using FFT as in Ref. 16 and set to 2.3 μm by stretching the preparation accordingly using the XYZ micrometer translation stage, to which the servomotor was attached. This sarcomeric length was used as it is within the range that mouse diaphragm muscle functions (44). To standardize force generation between muscle preparations, the cross-sectional area was calculated from the diameter assuming a circular geometry (1, 16, 18, 38). The average length (L_s) of the preparations used in this study was 2.9 ± 0.1 mm and the average cross-sectional area was 0.049 ± 0.002 mm^2. At each pCa, steady-state isometric force was measured, as was the rate of isometric tension redevelopment (k_{tr}) following rapid (< 4 L_s/S) release-restretch (15% L_s) of the preparation (18). Figure 1*D* is a sample trace of a force pCa curve generated by a preparation from a sham mouse. Throughout the experiment, Brenner cycling was used to maintain functional stability (6). Figure 1*E* is the force trace used to calculate the k_{tr} for a preparation from the sham mice at pCa 5.0.

Analysis. Each force-pCa curve was fit with the Hill equation:

$$F = F_{max}\{1 + 10^{n_H(pCa - pCa_{50})^{-1}}\}^{-1}$$

where F_{max} is the force at high [Ca^{2+}], pCa_{50} is the pCa needed to achieve 50% of F_{max} (used here as a measure of the Ca^{2+} sensitivity of force), and n_H, the Hill coefficient, reflects the steepness of the relation. The reported values for each of these parameters represent the means of the values from the individual fits ± SE. The data produced by the k_{tr} protocol describing the increase in force following the rapid release restretch was well fit by a single-exponential equation. The calculated error values, used as a goodness-of-fit indicator, were within an acceptable range. In addition, each data fit was examined by eye to confirm a good fit.

Myosin heavy chain isoform content. To determine myosin heavy chain isoform composition, diaphragm muscle was prepared for SDS-PAGE. An entire lobe of a diaphragm was solubilized for this work so that the data were well representative of the multiple fiber composition of the diaphragm muscle. The myosin isoforms in these samples were separated as previously described (66) using a miniVE system (GE Healthcare, Burlington, ON). The stacking gel was 4% acrylamide (pH 6.8) and the separating gel contained 7% acrylamide (pH 8.8) with 30% glycerol (vol/vol). Gels were run for ~20 h at 4°C. Gels were stained with Coomassie, imaged using a Bio-Rad Chemi-Doc Scanner, and band densities were quantified with ImageJ (National Institutes of Health). Each myosin heavy chain band was expressed as a percent of the total amount of myosin that was quantified in each lane. Before analysis percentage data was first logit transformed.

The identity of each myosin band was confirmed using tandem mass spectroscopy completed at the Advanced Protein Analysis Center at Sick Kids Hospital (Toronto, ON) using an Applied Biosystems/MDS Sciex API QSTAR XL Pulsar MALDI QTOF mass spectrometor. All MS/MS samples were analyzed using Mascot (Matrix Science, London, UK; version Mascot) as in Alderman et al. (3). Scaffold (version Scaffold 4.1, Proteome Software, Portland, OR) was used to validate MS/MS based peptide and protein identifications. Peptide identifications were accepted if they could be established at greater than 95.0% probability as specified by the Peptide Prophet algorithm (26). Protein identifications were accepted if they could be established at greater than 95.0% probability and contained at least 5 identified peptides. Protein probabilities were assigned by the Protein Prophet algorithm (40).

Phosphorylation detection. An aliquot of the protein samples from the diaphragm preparations used for the myosin quantification was utilized for phosphorylation detection as described previously (16). In brief, samples were separated on 12% SDS-PAGE gels using a miniVE system (GE Healthcare) and stained with Pro-Q Phosphoprotein stain following the manufacturer's instructions (Molecular Probes, Burlington, ON). Gels were imaged using a Bio-Rad Chemi Doc MP fluorescent scanner. All gels were then stained for total protein using SYPRO-ruby following the manufacturer's instructions (Molecular Probes) and reimaged.

Western blotting and analysis of myofilament proteolysis. To identify the myofilament proteins in mouse diaphragm muscle, SDS-PAGE and Western blotting were used. Mouse diaphragm myofilament proteins were separated by 12.5% SDS-PAGE as described above without glycerol. The SDS-PAGE gel was transferred onto a Trans-Blot Turbo Midi Nitrocellulose membrane (Bio-Rad Laboratories, Mississauga, ON) using a Trans-Blot Turbo semi-dry transfer unit (Bio-Rad Laboratories). Primary antibodies were used against desmin [D76, Developmental Studies Hybridoma Bank (DSHB)]; actin [5C5, Sigma Aldrich (Sigma), Oakville, ON]; TnT (CT3, DSHB; and JLT12; Sigma); Tm (CH1; Sigma); MLC 1 and 2 (T14; DSHB); ssTnI [MYNT; gift from Dr. N. Matsumoto (PMID 15833785)]; and fsTnI (F23; International Point of Care, Toronto, ON). Two TnT Abs were used so that all isoforms of TnT could be identified. In the phosphorylation analysis the signals for the identified bands were summed. The secondary antibody was a goat anti-mouse IgG conjugated to alkaline phosphatase (Jackson immunohistochemistry, Burlington, ON). Western blots were imaged using a ChemiDoc MP System (Bio-Rad Laboratories).

To investigate myofilament proteolysis, frozen whole diaphragm muscles were homogenized in 100 mM Tris (pH 7.8) with 50 mM NaF, 0.25 mM Na_3VO_4 and protease inhibitors (100 μM phenylmethylsulfonyl fluoride, 10 μM leupeptin, 2 μM pepstatin A, 1 μM aprotinin and 25 mM EDTA). Total protein concentration was determined by the Lowry assay before preparation of protein samples in Laemmli buffer with 25 mM dithiothreitol (DTT). The quantities of intact actin, tropomyosin, TnT, and fast and slow TnI were determined by densitometry. The specificity of all antibodies had been previously confirmed (51).

Statistics. Values presented are means ± SE. Statistical analyses were completed using GraphPad (Prism 6, GraphPad Software, LaJolla, CA). Single-factor ANOVA and Tukey's post hoc tests were used to test statistical differences between data from the treatment groups and the sham group. Significance was determined at $P < 0.05$.

RESULTS

Transverse aortic constriction and acute myocardial infarction induce cardiac remodeling and diaphragmatic myopathy. In this study, we used two mouse models to investigate the effects of HF on the development of myofilament contractile dysfunction of the diaphragm. Pressure-overload HF was induced by TAC, whereas HF caused by myocardial infarction was induced by permanent ligation of the left anterior descending coronary artery. Data from sham-operated animals, at all time points and between surgical models, were indistinguishable and were therefore combined and used to compare against data from experimental groups.

To ensure the establishment of HF, histomorphometrics, invasive hemodynamics, and echocardiography were measured at 2 or 18 wk of TAC and 18 wk post AMI (Fig. 2). Using histology cross sections of the heart at the apex, midpapillary, and base regions, ligation of the LAD resulted in a left ventricle infarct area of 53.4% ± 3.5% by 2 wk post-AMI; by 18 wk post-AMI, remodeling resulted in dilation of the infarct area to 62.45% ± 2.54%. As expected, histological and morphometric analysis revealed myocardial hypertrophy (Fig. 2, *B–D*), respectively, in all treatment groups. Echocardiography revealed chamber dilation by 18 wk (Fig. 2, *E* and *F*) and a progressive loss of contractile function in all groups indicated by a reduction in ejection fraction (Fig. 2*G*) and cardiac output (Fig. 2*H*).

We next evaluated the effects of HF on diaphragm structure and function. Histological assessment of diaphragm tissue (Fig. 2*I*) reveals a significant reduction in average myocyte cross-sectional area (CSA) (Fig. 2*J*) in 18 wk TAC and AMI but not 2 wk TAC. Interestingly, the development of atrophy did not impair the intrinsic ability of the diaphragm to generate force when normalized to muscle physiological cross-sectional area, as maximal in vitro force production was not reduced in any groups (Fig. 2*K*). Maximal in vitro force production is, in large part, reflective of the fiber type composition of the tissue. For CD-1 mice, maximum in vitro force reported here is similar to other published work (5, 61). Interestingly, 2 wk TAC resulted in enhanced in vitro force production, which has previously been attributed to alterations in calcium cycling (33). Similar to patients with HF, inspiratory pressure generation at baseline was increased following application of pressure-overload (Fig. 2*L*). In summary, these data indicate that during the early

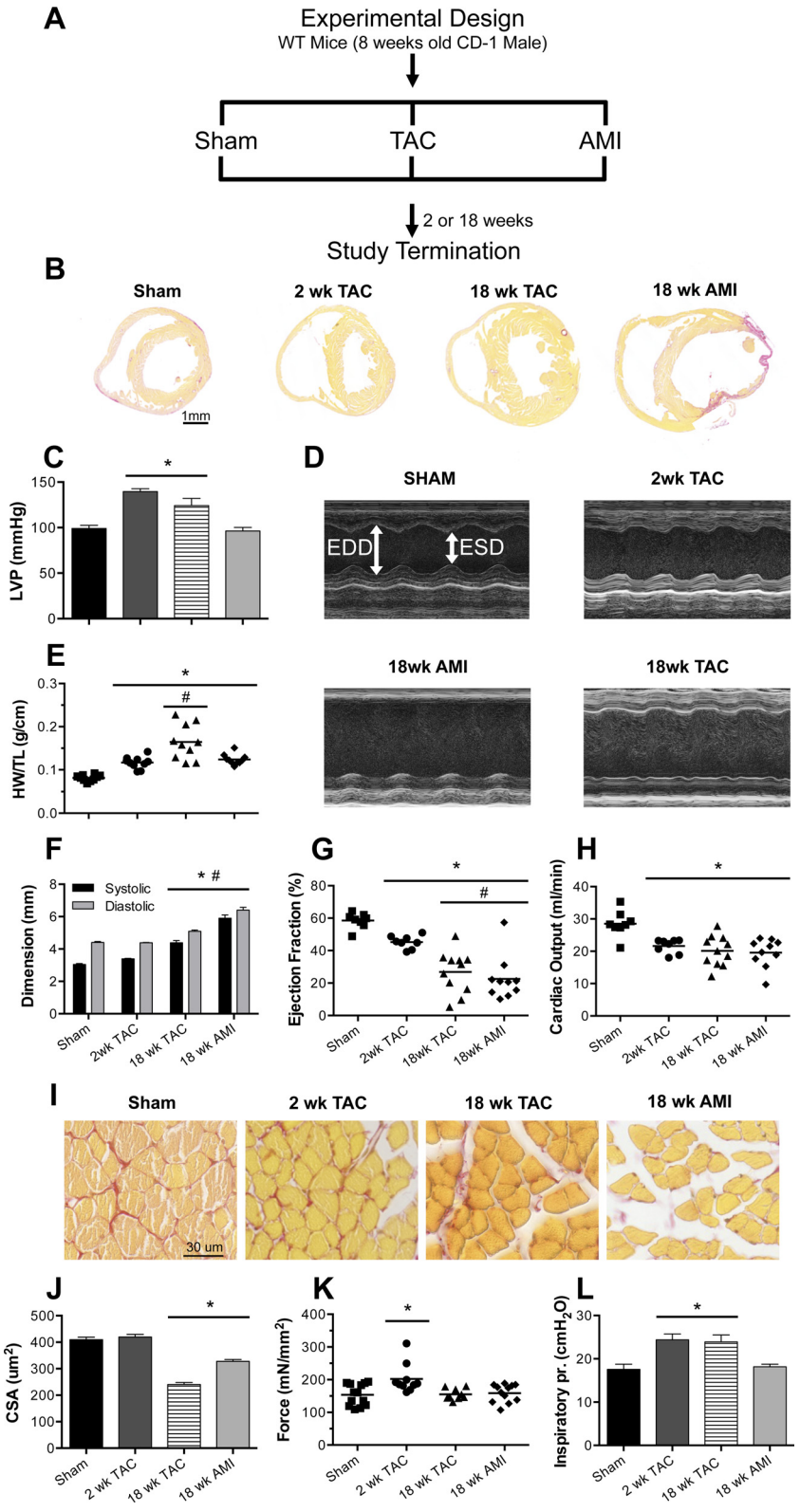

Fig. 2. Differences in the morphology and function of the heart and diaphragm during development of heart failure (HF) caused by either transverse aortic constriction (TAC) or acute myocardial infarction (AMI). *A*: experimental design. WT, wild type. *B*: TAC and AMI induce cardiac hypertrophy/remodeling. *C*: elevated left ventricular pressure (LVP) occurred only in the TAC model. Elevated heart weight/tibial length (HW/TL; *E*) confirms cardiac hypertrophy in all groups while echocardiography (*D*) demonstrates impaired cardiac contractility and progression into HF, as indicated by elevations in systolic and diastolic left ventricular dimensions (*F*) and reductions in ejection fraction (*G*) and cardiac output (*H*). Histological analysis of transverse sections of diaphragm tissue (*I*) reveals a significant reduction in average myocyte cross-sectional area (CSA; *J*), while maximum in vitro diaphragm force production is higher in the preparations from the 2 wk TAC but identical to sham in the 18 wk TAC and 18 wk AMI group (*K*). Inspiratory pressure generation at baseline was increased following application of pressure-overload (*L*). Bars are mean ± SE. *Significance vs. sham, $P < 0.05$; #significance vs. 2 wk TAC, $P < 0.05$; as determined by ANOVA and Tukey's post hoc.

progression of HF, diaphragmatic atrophy developed with preserved in vitro contractile function.

Ca^{2+} activation of force generation by the chemically skinned myofilament preparations. The Ca^{2+} activation of force generation by the chemically skinned myofilament preparations from the sham and three treatment groups demonstrated a sigmoidal relationship with force reaching an asymptote by pCa 5.2 (Fig. 3*A*). There was no difference in the maximum Ca^{2+}-activated force generated by the myofilament preparations from the sham group and those from the 2 wk

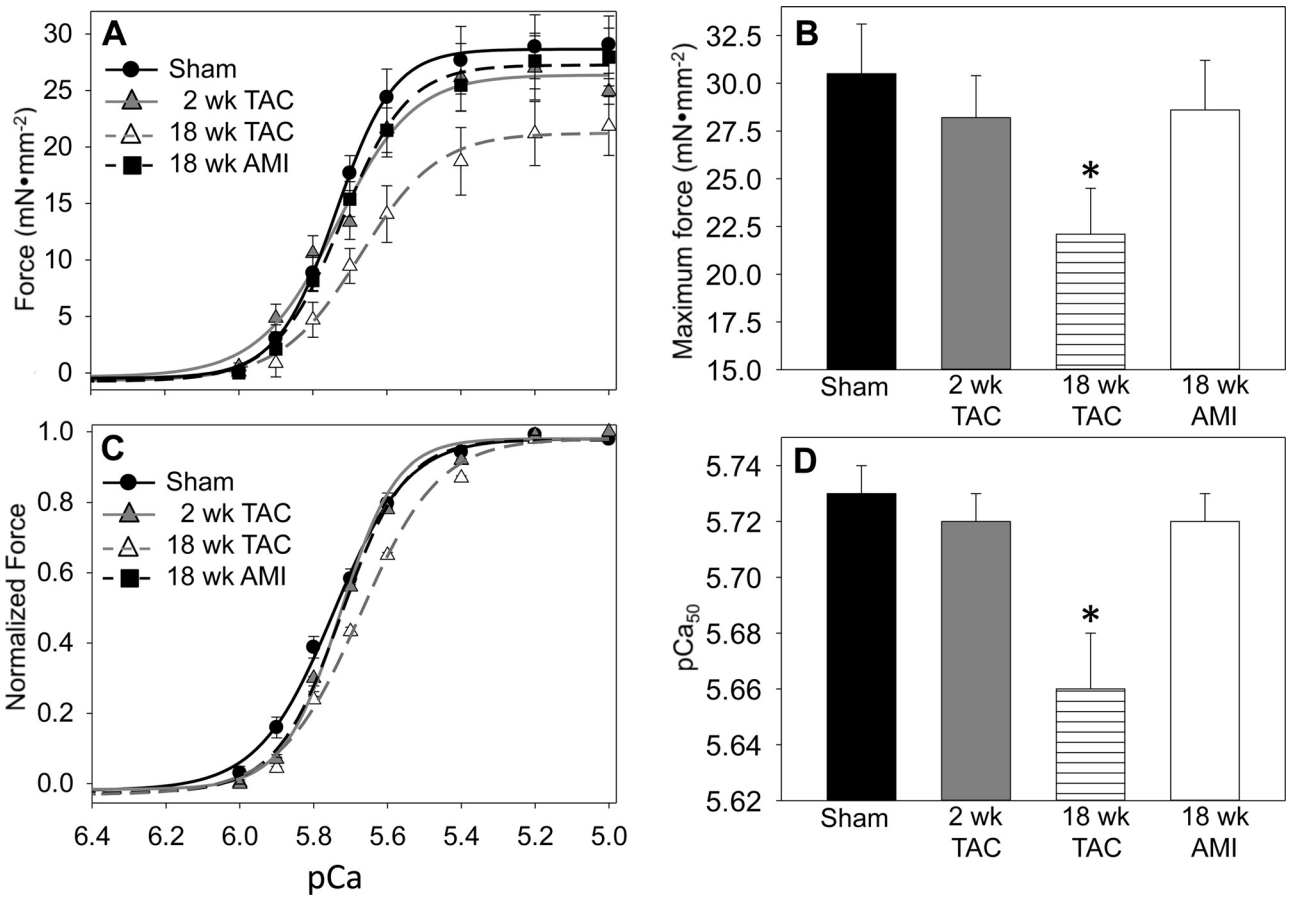

Fig. 3. Ca^{2+}-activated force and the Ca^{2+} sensitivity of force generation by diaphragm muscle preparations is reduced 18 wk post transverse aortic constriction (TAC). *A*: actual Ca^{2+}-activated force generated by diaphragm preparations measured as mN/mm^2. *B*: maximum Ca^{2+} activated force. *C*: normalized Ca^{2+}-activated force generated by diaphragm preparations. *D*: Ca^{2+} concentration, in pCa, at half-maximum force generation (pCa_{50}). For *C*, force measurement was normalized by setting maximum force generated for each experiment to 1. For sham, $N = 17$, where N is the number of preparations; for 2 wk TAC group, $N = 19$; for 18 wk TAC group, $N = 17$; for 18-wk AMI group, $N = 20$. The preparations were dissected from the diaphragms of 8 mice per experimental group. Values are means ± SE; some error bars are smaller than the symbols. The curves generated by fitting the data with the Hill equation have been added to *A* and *C* for comparison against the data points. On *A, B*, and *D*: *significant differences between the preparations from the 18 wk TAC and sham for the displayed parameter. On *A* these differences are at each experimental pCa indicated. 2 wk TAC, 2 wk post transverse aortic constriction; 18 wk TAC, 18 wk post transverse aortic constriction; 18 wk AMI, 18 wk post acute myocardial infarction.

TAC group and the 18 wk AMI group (Fig. 3*B*). However, the myofilament preparations from the 18 wk TAC group generated less force when maximally activated than those from the sham group (Table 1 and Fig. 3*B*).

The Ca^{2+} sensitivity of force generation, measured as the Ca^{2+} concentration (expressed as a pCa), at half-maximum force was significantly less in the myofilament preparations from the 18 wk TAC group compared with those from the sham group, the 2 wk TAC group, and the 18 wk AMI group (Table 1, Fig. 3, *C* and *D*). This is illustrated in Fig. 3*C*, where the force-pCa curve of the 18 wk TAC group is shifted to the right of those for the sham, 2 wk TAC, and 18 wk AMI group. There was no difference in the Ca^{2+} sensitivity of the myofilament preparations from the sham group and those from the 2 wk TAC group and the 18 wk AMI group (Table 1 and Fig. 3*D*). The cooperativity of the force/pCa curve, measured as the

Table 1. *Dependent variables of Ca^{2+} activation from diaphragm preparations from sham mice, 2 wk TAC mice, 18 wk TAC mice, and 18 wk AMI mice*

Group	F_{max}, mN/mm^2	$F_{5.7}$, mN/mm^2	pCa_{50}	n_H	Passive Force, mN/mm^2	k_{tr} at F_{max}, s^{-1}
Sham	30.5 ± 2.6^a	17.7 ± 3.6^a	5.73 ± 0.01^a	4.6 ± 0.3^a	1.8 ± 0.3^a	5.1 ± 0.2^a
2 wk TAC	28.1 ± 2.2^{ab}	13.4 ± 1.7^a	5.72 ± 0.01^a	6.3 ± 0.3^b	0.9 ± 0.1^{bc}	4.2 ± 0.3^b
18 wk TAC	22.1 ± 2.4^b	9.5 ± 1.7^b	5.66 ± 0.02^b	4.1 ± 0.3^a	1.5 ± 0.3^{ab}	4.0 ± 0.3^{bc}
18 wk AMI	28.6 ± 2.6^{ab}	15.4 ± 1.6^a	5.72 ± 0.01^a	5.3 ± 0.2^c	0.8 ± 0.1^c	3.5 ± 0.2^c

Values are means ± SE. TAC, transverse aortic constriction; AMI, acute myocardial infarction; F_{max}, maximum force generated; $F_{5.7}$, force generated at pCa 5.7; pCa_{50}, Ca^{2+} concentration, measured as pCa, at half-maximum force generation; n_H, Hill coefficient; Passive force, passive tension at pCa 9.0; k_{tr} at F_{max}, rate of force generation at maximum activation. Values within the same column that share a superscript (a, b, and c), are not significantly different from each other ($P < 0.05$).

Hill coefficient, was greater for the preparations from the 2 wk TAC group and 18 wk AMI group compared with those from the sham and 18 wk TAC group (Table 1). This means that an increase in cytosolic Ca^{2+} concentration would cause a greater change in force production by these diaphragms than a similar pCa change in the myofilament preparations from either the sham or 18 wk TAC group. There was no difference in the Hill coefficient of the force-pCa curves for the preparations from the sham group and the 18 wk TAC group (Table 1).

The closest pCa to the pCa_{50}, calculated using the Hill equation (Table 1), to those at which force was measured in our protocol was pCa 5.7. Comparison of the force generated by myofilament preparations at pCa 5.7 from all groups revealed that less force was generated in the preparations from the 18 wk TAC group than those from the sham group as well as the 2 wk TAC and 18 wk AMI group ($P < 0.05$, Table 1). In addition, the amount of force generated by the preparations from the 18 wk TAC group was significantly less than that generated by the preparations from the sham group at all experimental pCa except for pCa 5.9 and pCa 6.0. This demonstrates that the force-generating capacity of the 18 wk TAC diaphragmatic myofilaments was impaired within the physiological range of cytosolic Ca^{2+}. The passive force of the myofilament preparations from the sham group was the same as those from the 18 wk TAC group but greater than that of preparations from either the 2 wk TAC group or 18 wk AMI group (Table 1). Additionally, there was no difference in the passive force of the myofilament preparations from the 2 wk TAC group and those from the 18 wk AMI group.

Ca^{2+} dependence of k_{tr}. The k_{tr} at maximum activation was greater in the diaphragmatic myofilament preparations from the sham group compared with those from the 2 and 18 wk TAC and the 18 wk AMI groups (Table 1). To examine how this characteristic is influenced by Ca^{2+} concentration, the dependence of k_{tr} on $[Ca^{2+}]$ was plotted on top of the standardized steady-state force-pCa relationship (Fig. 4). In the myofilament preparations from the sham group, k_{tr} increased with pCa in parallel with Ca^{2+}-activated force and reached an asymptote close to maximum force generation (Fig. 4*A*). However, in the myofilament preparations from the 2 and 18 wk TAC and the 18 wk AMI groups, k_{tr} initially increases with pCa but then reaches an asymptote before force generation reaches a maximum (Fig. 4). The maximum k_{tr} values reached in the three experimental groups were ~80% of that generated in the sham preparation. This indicates that the rate of cross-bridge cycling was becoming disconnected from the Ca^{2+} activation of iso-

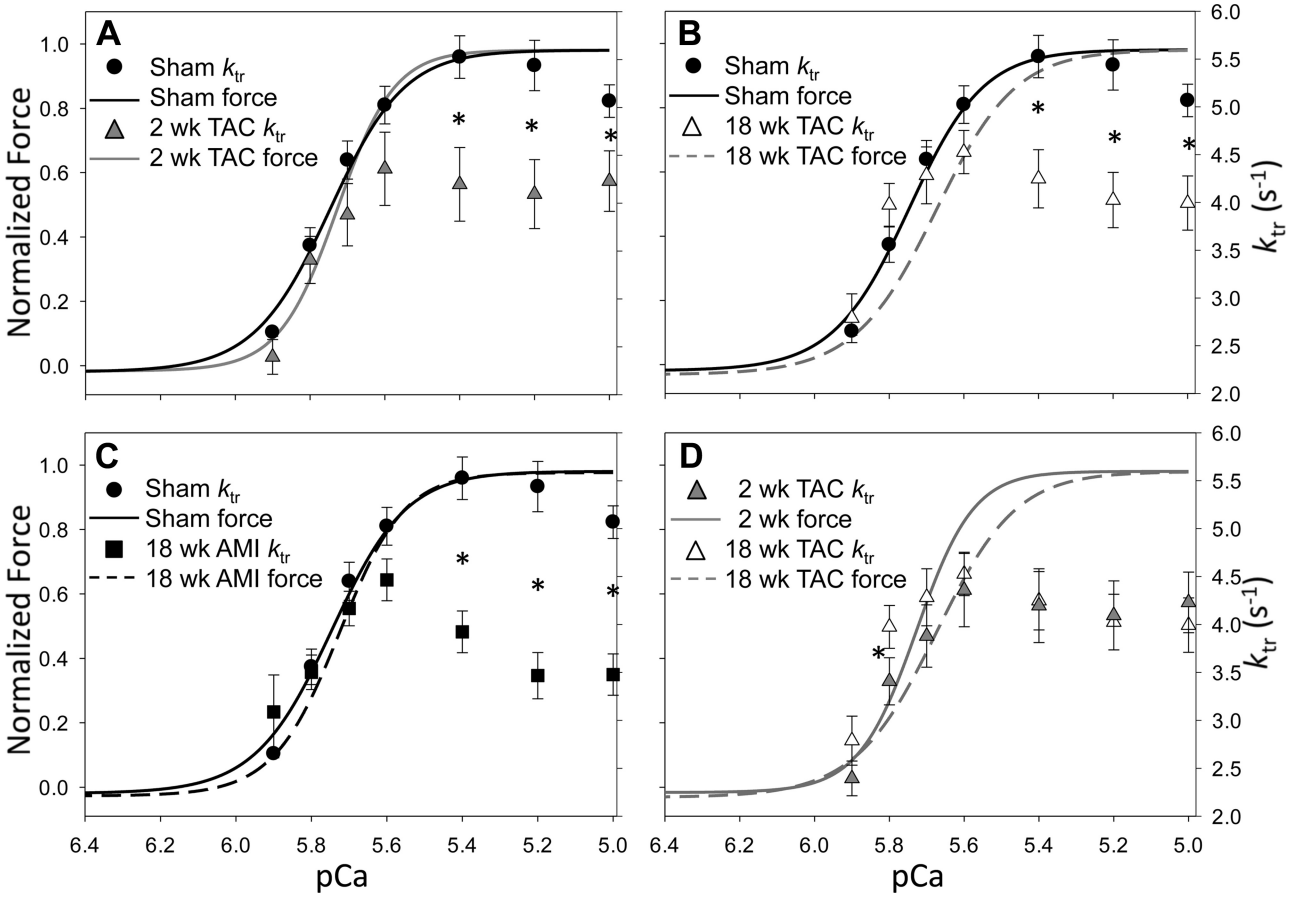

Fig. 4. The influence of Ca^{2+} concentration on steady-state isometric force development and k_{tr}. Plots compare sham and the 2 wk TAC group (*A*), sham and the 18 wk TAC group (*B*), sham and the 18 wk AMI group (*C*), and 2 wk TAC group and the 18 wk TAC group (*D*). Force is standardized to the maximum within each treatment. For sham, $N = 17$, where N is the number of preparations; for 2 wk TAC group, $N = 19$; for 18 wk TAC group, $N = 17$; for 18 wk AMI group, $N = 20$. The preparations were dissected from the diaphragms of 8 mice per experimental group. Values are means ± SE. The curves were generated by fitting the standardized force data with the Hill equation. Significant differences in k_{tr} between groups at the same pCa are indicated on each panel: $*P < 0.05$. All scales are identical between all panels.

meric force generation. In the myofilament preparations from the 18 wk TAC and 18 wk AMI group, k_{tr} was found to decline once this asymptote was reached. In the myofilament preparations from all treatment groups, the k_{tr} generated, once maximum force was reached, was significantly less than that in the sham preparations at the same pCa (Fig. 4). Comparison of the k_{tr}-pCa curves from the 2 wk TAC and 18 wk TAC groups revealed the force-pCa curve of the 18 wk TAC group was shifted to the right of the 2 wk TAC group and that k_{tr} was significantly higher in the 18 wk TAC group at pCa 5.8 (Fig. 4*D*). This indicates that cross-bridge cycling was higher at lower levels of Ca^{2+} activation/force generation in the 18 wk TAC group compared with the 2 wk TAC group. This also suggests that the change in Ca^{2+} sensitivity and force generation in the preparations from the 18 wk TAC group may be independent of the change in cross-bridge cycling.

Relationship between force production and the rate of cross-bridge cycling. To determine if the Ca^{2+}-dependent increases in k_{tr} resulted in an increase in the number of force-producing cross-bridges, the data in Fig. 4 were replotted as k_{tr} vs. relative force production (Fig. 5), and force measurements were standardized to maximum force generated by the sham preparations. This allowed for the averaged k_{tr} data from each treatment group to be compared at similar levels of force production independent of $[Ca^{2+}]$. This replotting demonstrated that in the sham group, k_{tr} increased with steady-state force production until an asymptote is reached in force. In the 2 wk TAC preparations, k_{tr} initially increased proportional to the force, and the rate was no different from that from an equal force produced in the sham group. However, the rate of cross-bridge cycling began to slow once force reached 50% of the relative maximum. When maximum force generation is achieved in the myofilament preparations from the 2 wk TAC, at 82% of relative maximum, k_{tr} is 73% that of the sham for the same level of force generation (Fig. 5*A*). This indicates that the amount of force being generated per cross-bridge is increasing and could be due to the cross-bridge remaining bound for a longer period of time. Such a change in cross-bridge dynamics would result from either a decrease in the rate of Ca^{2+} disassociation from the Tn complex or a slowing in the move-

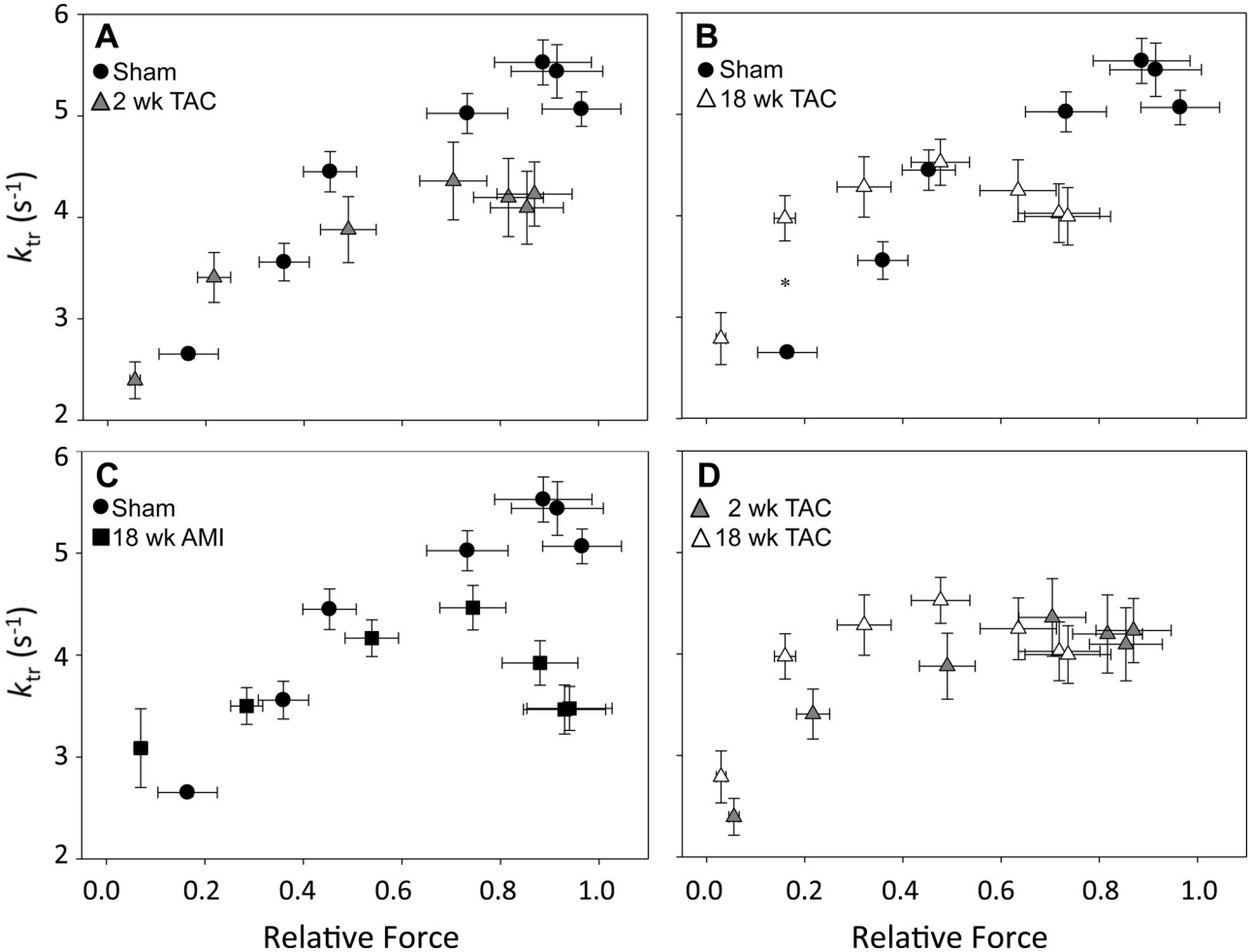

Fig. 5. The relationship between k_{tr} and steady-state force as pCa is varied. Data from Fig. 2 were replotted against steady-state isometric force normalized with the average maximum force generated by the sham preparations. This allows for the k_{tr} data from each treatment group to be compared at similar levels of force production independent of $[Ca^{2+}]$. Plots compare sham and the 2 wk TAC group (*A*), sham and the 18 wk TAC group (*B*), sham and the 18 wk AMI group (*C*), and 2 wk TAC group and the 18 wk TAC group (*D*). For sham, $N = 17$, where N is the number of preparations; for 2 wk TAC group, $N = 19$; for 18 wk TAC group, $N = 17$; for 18 wk AMI group, $N = 20$. The preparations were dissected from the diaphragms of 8 mice for each experimental groups. Values are means ± SE. All scales are identical between all panels. Significant differences in k_{tr} between groups at the same level of force generation are indicated on each panel: $^*P < 0.05$.

ment of the myosin head. As ATP was not limiting in the experiments, fatigue was not an issue. In the myofilament preparations from the 18 wk TAC group, k_{tr} was significantly greater than in the preparations from the sham group at low levels of force production but they reached their maximum at only ~50% of the maximum standardized force (Fig. 5*B*). This suggests that at low levels of force production, at physiologically relevant Ca^{2+} concentrations, the rate of cross-bridge cycling is faster in the 18 wk TAC group but the amount of force per cross-bridge is lower. At higher levels of force production, the rate of cross-bridge cycling in the 18 wk TAC preparation was also decreased. At maximum activation, the preparations from the 18 wk TAC group generated 72% of the force generated by sham preparations when maximally activated. The rate of cross-bridge cycling in the 18 wk TAC preparations at this level of force production is ~78% that of the sham at the same level of force production (Fig. 5*B*). In the preparations from the 18 wk AMI group, k_{tr} increased with force generation as in the sham preparations; however, k_{tr} reached an asymptote at ~75% maximum standardized force and then begins to rapidly decrease as force generation increased. The maximum force produced by these preparations was ~94% that of the sham group at maximum levels of activation but the rate of cross-bridge cycling at this level of force production was only ~66% that for the same amount of force production in the sham preparations (Fig. 5*C*). This reduced rate of cross-bridge cycling would translate into a decrease in the rate of contraction and indicates that, as in the preparations from the other treatment groups, the amount of force generated per cross-bridge was increasing. Finally the rate of cross-bridge cycling was higher at a similar level of force generated at physiological levels of Ca^{2+} activation in the 18 wk TAC group compared with the 2 wk TAC group. This indicates that less force was being generated per cross-bridge (Fig. 5*D*).

Protein phosphorylation. There were five sarcomeric proteins that were differentially phosphorylated between the groups (Fig. 6, *A–J*). In the 2 wk TAC group the level of β-TM and TnT phosphorylation was higher in the preparations from the 2 wk TAC diaphragms compared with sham while the level of MLC1 and MLC2 phosphorylation was lower compared with sham (Fig. 6*K*). In the preparations from the 18 wk TAC group the phosphorylation level of desmin, TnT, MLC-1 and MLC-2 was significantly lower compared with the shams (Fig. 6*K*) with the level of TnT and MLC-2 phosphorylation being undetectable (Fig. 6*K*). The level of desmin phosphorylation was higher in the preparations from 18 wk AMI group compared with the preparations from the sham group. Myosin heavy chain (MyHC) was phosphorylated in all samples measured, but there was no difference between experimental and sham groups (Fig. 6*K*).

Myosin heavy chain (MyHC) composition. Three distinct MyHC bands were identified (Fig. 7A). Tandem MS indicated that the top band contained MyHC-2x and MyHC-2a, the middle band MyHC-2b, and the lower band MyHC-1b slow. Previous work with mouse diaphragm supports these identifications (2). The only change in myosin composition, relative to that in preparations, was in the 18 wk TAC group. This was a decrease in the percent composition of MyHC-2b and an increase in the percent composition MyHC-2x and MyHC-2a ($P < 0.05$) (Fig. 7*B*).

Myofilament proteolysis. Cardiac or skeletal muscle TnI is one of the most sensitive myofilament protein to undergo degradation when proteolysis occurs in response to stress (49–51, 65). Thus, to investigate proteolysis of myofilament proteins, actin (α and β), TM, TnT, and fast and slow TnI were investigated in sham, 18 wk TAC, and 18 wk AMI diaphragm samples. With short Western blot exposures, no changes in quantity of these proteins were identified between sham, TAC, or AMI samples (Fig. 8). For further confirmation, blots were subjected to prolonged exposures; no proteolytic fragments were observed (data not shown).

DISCUSSION

The goal of this study was to understand the initial changes in diaphragm myofilament function in response to either pressure-overload-induced HF, or myocardial infarction-induced HF. The results demonstrate specific and progressive complex alterations in myofilament function and phosphorylation status in diaphragm preparations that are model specific and occur quickly after induction of pressure-overload HF (see Table 2). Specifically, our novel findings are *1*) during the early phase development of HF, in vitro diaphragmatic function is preserved while myofilament function is impaired; *2*) myofilament dysfunction occurs before evidence of diaphragm atrophy; *3*) myofilament dysfunction was evident by a decrease in the rate of cross-bridge cycling in all groups and *4*) with decreases in Ca^{2+} sensitivity of force generation and the force generating capacity at 18 wk TAC; *5*) a reduction in myofilament phosphorylation of desmin, fsTnT, MLC1, and MLC2, at 18 wk TAC; and *6*) the relative proportion of MyHC 2b was lower in 18 wk TAC while that of MyHC 2a + MyHC 2x was correspondingly greater. As these alterations in diaphragmatic myofilament function occurred before any evidence of diaphragm atrophy or impairments of in vitro function suggests that loss of myofilament function along with alterations in phosphorylation status may be the incipient event that leads to fiber type shifting, atrophy, and whole muscle dysfunction.

Diaphragm myofilament function during development of heart failure. The animals in the TAC and AMI groups both exhibited cardiac dysfunction at 18 wk. This was evident by the ventricular dilation, loss of cardiac contractile function, and reduction in ejection fraction characterized in both groups. The development of heart failure did not cause overt diaphragmatic dysfunction as demonstrated by the in vitro measurements of force generation. In fact, there was an increase in the maximal in vitro force measured in the 2 wk TAC group. The development of heart failure did alter the function of the isolated myofilaments, suggesting that compensatory changes occurring elsewhere within the muscle (e.g., SERCA function or calcium handling/release/uptake) were also occurring. There are also differences in how myofilament function is affected by the two heart failure models. For example, the contractile function of the diaphragm myofilaments from the 18 wk AMI group was not as affected as those from the TAC group at this time point. While there was a reduction in the rate of cross-bridge cycling at high levels of Ca^{2+} activation in the preparations from the AMI group at 18 wk, there was no loss of Ca^{2+} sensitivity or force-generating capacity as there was in the preparations from the TAC group. This variation in functional response indicates that the myofilaments are differen-

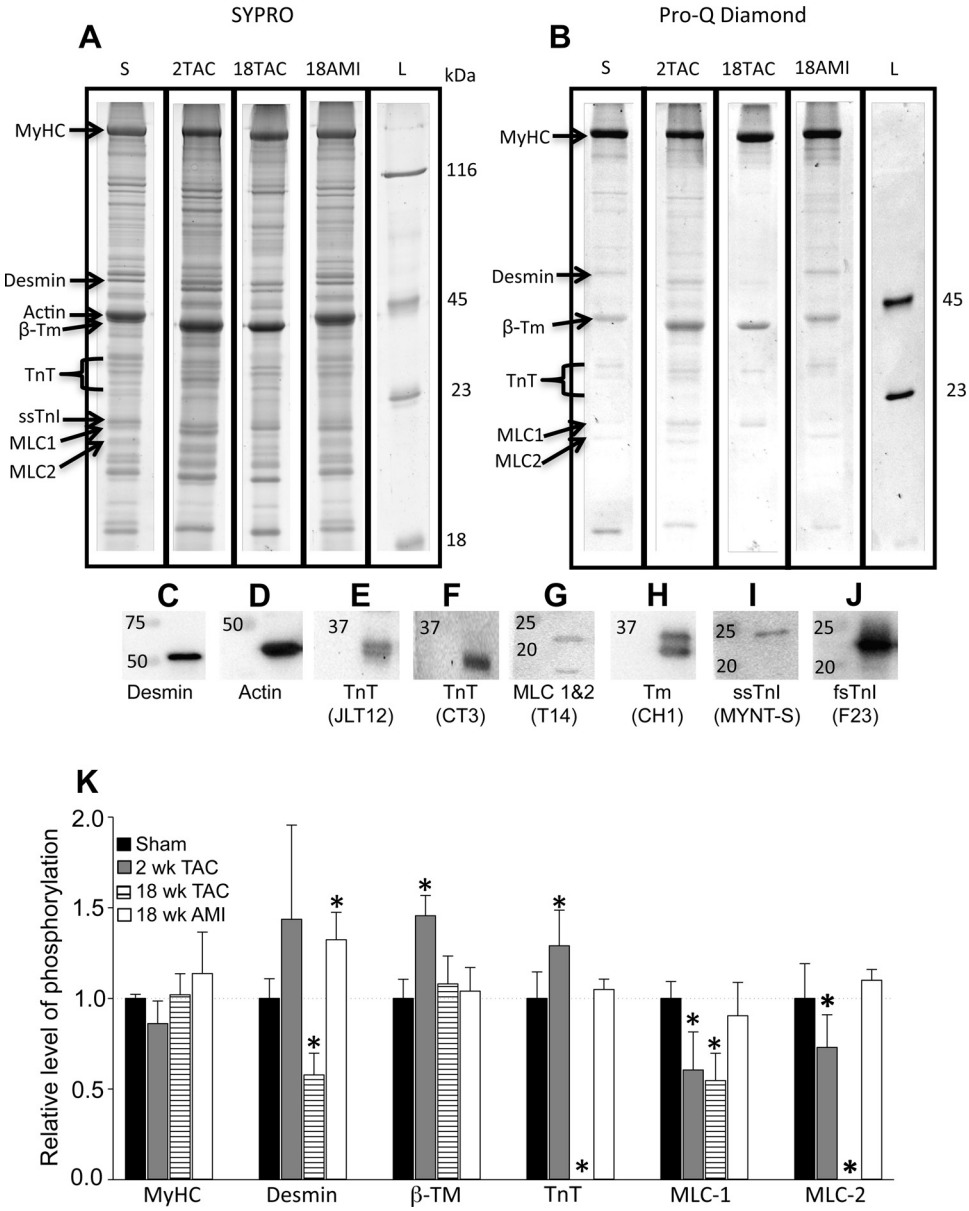

Fig. 6. The influence of early stage heart failure on the mouse diaphragm proteome. *A*: representative Sypro Ruby-stained and ProQ-Diamond-stained gels indicating total protein and phosphorylated proteins, respectively, in the diaphragm muscle from mice in the sham group, 2 wk TAC group, 18 wk TAC group, and 18 wk AMI group. The positions of myosin heavy chain (MyHC), desmin, actin, β-tropomyosin (β-TM), troponin T (TnT), slow skeletal TnI (ssTnI), myosin regulatory light chain 1 (MLC1), and myosin regulatory light chain 2 (MLC2) are indicated on the gel. Lane L is the peppermint stick weight ladder (Molecular Probes). *B*: representative ProQ-Diamond-stained gels indicating phosphorylated proteins in the diaphragm muscle from mice in the sham group, 2 wk TAC group, 18 wk TAC group, and 18 wk AMI group. Lane L is the peppermint stick weight ladder with two phosphorylated proteins at 23.6 kDa and 45 kDa visible. *C–J* are representative Western blots of the diaphragm muscle samples using the antibodies for the proteins indicated. fsTnI, fast skeletal TnI. *K*: relative level of phosphorylation of the contractile proteins. The mean of the phosphorylation level of each protein in the sham samples was standardized to equal 1, and then all values shown from the different treatments are relative to this value. *N* is 4 for each plotted mean where an *N* is the lobe of diaphragm from a single mouse. Difference between treatment and control values in the same panel: $*P < 0.05$. All values are means ± SD. The level of phosphorylation for each protein in each sample was standardized with the density of the actin band in the same lane following Sypro staining (Molecular Probes) for total protein.

tially affected in the 2 models. This difference is also reflected in the relative levels of myofilament protein phosphorylation between the preparations from the 18 wk TAC and 18 wk AMI groups.

The steady-state force generated by striated muscle is determined by the number of cycling cross-bridges (6a, 6c). The rate of force redevelopment following release/restretch (k_{tr}) is thought to reflect cross-bridges transitioning between weakly attached states and force-generating states (6b). In skeletal muscle, at submaximal levels of activation, when Ca^{2+} is limited, k_{tr} is regulated by the Ca^{2+}-dependent interactions between the components of the thin filament (38). At saturating levels of Ca^{2+}, when skeletal fibers are maximally activated, k_{tr} is determined by the intrinsic rate of cross-bridge cycling (19). It therefore changes in the interaction between the thin and thick filaments that regulate k_{tr} during maximal activation (38). The reduction in k_{tr} at maximal activation in the preparations from the 2 wk TAC group indicates that myofilament function becomes impaired very early during the development of HF. Such a reduction in cross-bridge cycling would translate into reduced power development. However, at lower, more physiological levels of Ca^{2+} activation there were limited functional differences between the preparations from the 2 wk TAC group and sham. It is unlikely, then, that the alterations in myofilament function observed in the 2 wk TAC group would translate into a change in in vitro function.

The loss of Ca^{2+} sensitivity, force-generating capacity as well as the increase in k_{tr} at low, but physiological, levels of Ca^{2+} activation by the preparations from the TAC group at 18 wk, compared with the sham and 2 wk group, indicate that the function of diaphragm myofilaments is becoming increasingly compromised as the mice progress toward HF. These changes in function have the potential to cause muscle weakness and impair power generation by the muscle in vivo. Similar dysfunction has been reported for diaphragm preparations from mice with cancer cachexia (45). In this previous study, there

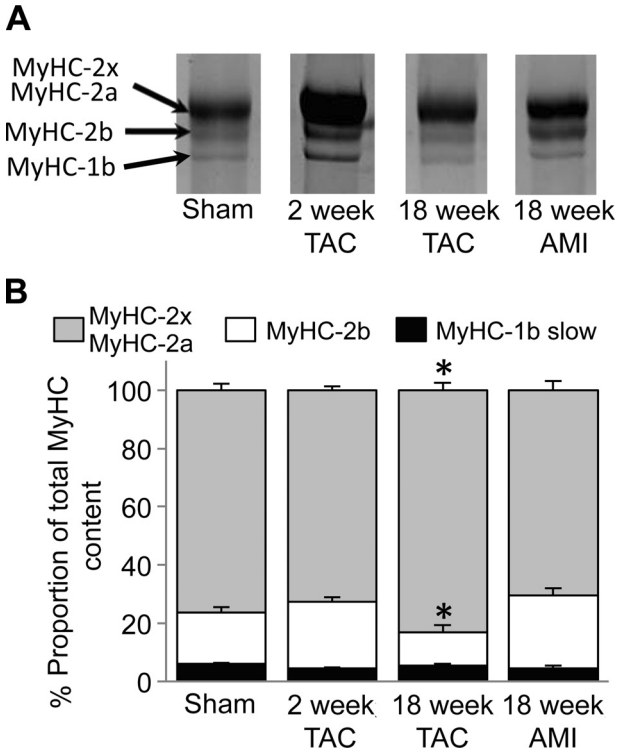

Fig. 7. Myosin heavy chain (MyHC) content of diaphragm muscle from the sham group, 2 wk transverse aortic constriction (TAC) group, 18 wk TAC group, and 18 wk acute myocardial infarction (AMI) group. *A*: representative images of separated myosin bands. Images are from two different gels. Protein samples from the sham group and 18 wk AMI group were run on one gel while samples from the 2 wk TAC and 18 wk TAC were separated on the second. The ladder shown was run on the first gel. *B*: MyHC isoform content of diaphragm samples from Sham, 2 wk TAC, 18 wk TAC, and 18 wk AMI, expressed as a percentage of total myosin. *N* is 6 for each plotted mean where an *N* is the lobe of diaphragm from a single mouse. Difference between treatment and control values: $^*P < 0.05$. All values are means ± SE.

was a reduction in the Ca^{2+} sensitivity of force generation, the force of contraction, as well as the k_{tr} in diaphragm preparations from cachexic CD2F1 mice (45). It was suggested that these changes in function were caused by a decrease in the number of strongly bound force-generating cross-bridges and/or less force was being generated per cross-bridge. The results of the current study are indicative of a similar cause for the loss of force generation in the preparations from the 18 wk TAC group. Critically, however, despite the loss of myofilament function, there was no reduction in the in vitro force production of the intact diaphragm preparation. For the force-generating capacity by the diaphragm to be maintained at pre-HF levels, compensatory changes would be required. This could include an increase in the number of myocytes activated per contraction or an increase in the concentration of excitatory Ca^{2+} released into the cell following an action potential. One factor that must be taken into account, however, when integrating the results of the myofilament studies with those of the in vitro force measurements is that the experimental temperatures were 12°C different. It is standard practice to complete measurements of myofilament function at 15°C as this ensures the integrity of the preparation and allows comparison with previous experiments (16, 18, 38).

Changes in myofilament protein phosphorylation. A detergent was used to remove cellular membranes in the myofilament preparations; therefore the observed changes in contractile function were due to changes in the function of the contractile proteins as opposed to calcium handling. One mechanism by which this can occur is through posttranslational modification (PTM) of the component myofilament proteins. The role of myofilament protein phosphorylation in regulating muscle function has been extensively studied in cardiac muscle (27, 32, 41, 52); however, much less is known of the role of protein phosphorylation in modulating the function of skeletal muscle (14). The greatest change in the phosphorylation state of the contractile proteins occurred in the 18 wk TAC preparations, the group with the greatest difference in diaphragmatic myofilament function, relative to sham. As the phosphorylation state of multiple proteins was decreased, the resultant functional change would be the net result of these multiple PTMs on myofilament function. For example, in fast skeletal muscle, the phosphorylation of MLC-2 increases the rate of cross-bridge cycling, and the Ca^{2+} sensitivity of force generation (20, 54, 59). It therefore follows that a reduction in MLC-2 phosphorylation would have the opposite effects. At high levels of myofilament activation these effects could, however, be altered by the decrease in the phosphorylation of TnT in the same muscle preparation. In cardiac muscle, the phosphorylation of cTnT at T203 causes a decrease in the rate of acto-

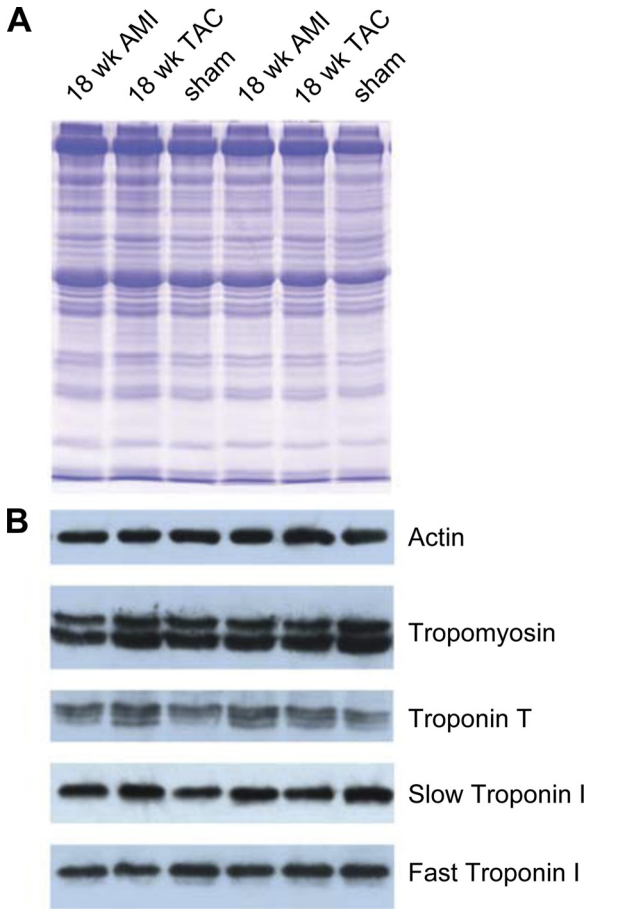

Fig. 8. Analysis of actin, TM, TnT, and fast and slow TnI content of diaphragm muscle from sham, 18 wk TAC, and 18 wk AMI groups for proteolytic degradation. *A*: representative Coomassie gel. *B*: Western blot probed for the presence of actin, Tm, TnT, and fast and slow TnI reveals no change in quantity of intact protein band as measured using densitometry.

Table 2. *Summary of morphological, in vitro functional, and compositional characteristics measured in the heart and diaphragm muscle from mice in the 2 wk TAC group, 18 wk TAC group, and 18 wk AMI group compared with the same preparations from the sham group*

	2 wk TAC	18 wk TAC	18 wk AMI
Heart morphology and function			
Myocardial hypertrophy	yes	yes	yes
Chamber dilation	no	yes	yes
Ejection fraction	nc	↓	↓
Cardiac output	nc	↓	↓
Diaphragm morphology and function			
Atrophy of myocytes	no	yes	yes
Interstitial fibrosis	no	yes	yes
In vitro force production	nc	nc	nc
In vitro myofilament function			
F_{max}	nc	↓	nc
$F_{5.7}$	nc	↓	nc
pCa_{50}	nc	↓	nc
k_{tr} at high forces	↓	↓	↓
k_{tr} at low forces	nc	↑	nc
Myofilament protein phosphorylation			
MyHC-*P*	nc	nc	nc
Desmin-*P*	nc	↓	↑
fsTnT-*P*	↓	↓	nc
β-TM-*P*	↑	nc	nc
MLC1-*P*	↑	↓↓	nc
MLC2-*P*	↓	↓↓	nc
Fiber type			
% MyHC 2b	nc	↓	nc
% MyHC 2x + MyHC 2a	nc	↑	nc
% MyHC 1b-slow	nc	nc	nc

"yes" indicates that the described condition was detected in the mice at time of sampling; "no" indicates that the described condition was not detected; an up arrow indicates a significant increase; a down arrow indicates a significant decrease; nc; no change; F_{max}, maximal Ca^{2+} activated force; $F_{5.7}$, force generated at pCa 5.7; pCa_{50}, Ca^{2+} concentration, measured as pCa, at half-maximum force generation; k_{tr} at high forces, rate of force generation at high forces; k_{tr} at low forces, rate of force generation at low forces; -*P*, phosphorylated; fsTnT, fast skeletal troponin T; β-TM, β-tropomyosin; MLC1, myosin light chain 1; MLC2, myosin light chain 2; % MyHC 2b, percentage of diaphragmatic muscle sample composed by myosin heavy chain 2b; % MyHC 2x + MyHC 2a, percentage of diaphragmatic muscle sample composed of myosin heavy chain 2x + myosin heavy chain 2a; % MyHC 1b-slow, percentage of diaphragmatic muscle sample composed of myosin heavy chain 1b slow.

myosin activity, Ca^{2+} sensitivity, and maximum force generation (57). Within fsTnT, the residue corresponding to cTnT T203 is fsTnT T156. At low levels of Ca^{2+} activation, where cross-bridge cycling is thought to be regulated by the Ca^{2+}-dependent interactions of the thin filament (38), the decrease in TnT phosphorylation in the preparations from the 18 wk TAC group could explain the slight, but not significant, increase in k_{tr} compared with shams' high pCa. An increase in k_{tr} would translate to the decrease in Ca^{2+}-activated force measured in these preparations at low levels of activation due to a reduction in the duty cycle of the myosin head. Interestingly, the level of TnT phosphorylation was higher in the preparations from the 2 wk TAC group but there was no difference in k_{tr} measured compared with sham at low levels of Ca^{2+} activation when measured at the same pCa. MLC-1 is also a critical regulator of muscle function through its interaction with the myosin head (37), and changes in its phosphorylation state have the potential to alter contractility. The same can be said for desmin. It is, however, not possible to predict the net effect of the dephosphorylation of each of the four myofilament proteins in the 2 wk and 18 wk TAC groups on muscle function. It is, however, not unreasonable to think that these changes are at least partially responsible for the observed functional changes in the myofilament preparations from the 18 wk TAC group.

Comparison of the differences in protein phosphorylation levels between the muscle samples from the different treatments reveals limited similarities. This indicates that there are likely different protein phosphorylation changes that can explain the decrease in k_{tr} characterized in all HF groups at higher levels of Ca^{2+} activation. However, one commonality between the preparations from the 2 and 18 wk TAC animals was a decrease in MLC-2 phosphorylation. The phosphorylation of MCL-2 increases the rate at which cross-bridges cycle from the non-force- to force-generating state (60). Such an effect increases k_{tr} at high levels of Ca^{2+} activation and is decreased by dephosphorylation (42).

While the level of MLC-1 and MLC-2 phosphorylation in the 2 wk TAC group was lower than that in the sham, this did not translate into a change in function. One explanation for this is that the increase in the phosphorylation of TnT compensated for this. The only change in phosphorylation detected in the 18 wk AMI group was an increase in desmin phosphorylation. This change could be responsible for the decrease in k_{tr} at high levels of activation by altering the interaction between the thin and thick filaments. Further studies are required to investigate manipulation of site-specific phosphorylation levels on myofilament function before we can begin to understand the complex changes in multiple phosphorylation sites in disease. Unlike cardiac myofilament proteins, which have been extensively studied in health and various disease states, the identification of skeletal myofilament PTM and their specific effect on regulating skeletal muscle function remains largely uninvestigated. Our work here shows skeletal myofilament phosphorylation status is complex and dynamic during development of HF. Further studies in this area are required to better understand how skeletal muscle function is acutely regulated by phosphorylation along with identification of the active kinases/phosphatases.

Fiber type changes. Skeletal muscle is composed of a spectrum of different muscle cell types, commonly referred to as muscle fiber types. The range of muscle fiber types allows for a muscle to respond to a variety of contractile demands with training and disease states altering the fiber composition of a muscle. The decrease in MyHC-2b and corresponding increase in MyHC-2x + MyHC-2a reported in the 18 wk TAC diaphragms indicates that the fiber profile of the diaphragm is shifting from a fast-twitch glycolytic to a fast-twitch oxidative phenotype. Probably the most notable respiratory muscle alteration in patients with HF is a relative shift in fiber composition that occurs in the opposite direction to that of limb muscles. In HF, there is a shift toward a greater proportion of type I (slow oxidative twitch) fibers in the diaphragm (8–10, 63, 64) while limb muscles show a greater proportion of type IIb (fast glycolytic twitch) fibers (12, 31, 34, 55, 56). Thus limb muscles and the diaphragm adapt in a qualitatively different manner in patients with HF. In this study, a modest change in the proportion of MyHC isoforms was only observed in the 18 wk TAC diaphragm and neither the 2 wk TAC nor the 18 wk

AMI. This can be explained based on diaphragm activity as we observed increases in resting respiratory pressure generation in only 2 wk and 18 wk TAC and not 18 wk AMI (Fig. 2*L*). The absence of changes in MyHC in the 2 wk TAC is likely because there was insufficient time for a shift in expression of MyHC to occur. Thus the chronic unrelenting increase in work of breathing, along with intrinsic changes in weakening the muscle, likely drove this adaptive change in fiber composition toward a more fatigue-resistant phenotype.

Previous studies have demonstrated that mechanical ventilation can increase the activity of calpain and caspase-3 in the diaphragm (for review, see 43). These are proteases that target the myofilaments leading to atrophy and diaphragm weakness (43). In the current study, no evidence of proteolysis was found in the myofilament proteins isolated from the diaphragm preparations from the 18 wk TAC and 18 wk AMI groups, nor was there loss of in vitro force generation in the 18 wk TAC and 18 wk AMI groups. Previous studies have reported that the proteolysis of myofilament proteins triggered by mechanical ventilation occurs in conjunction with a decrease in diaphragm in vitro function (25, 29, 39, 47, 48). Taken together our data suggest that myofilament proteolysis was not occurring in the diaphragms of either model of heart failure.

Conclusions and future perspectives. The results of this study indicate that early development of HF in mice, as a result of either a pressure overload or myocardial infarction, causes functional impairment of the diaphragm myofilament proteins. With TAC, myofilament dysfunction progressed from the decrease in k_{tr} at high levels of Ca^{2+} activation (>50% force generation) detected at 2 wk to the loss of Ca^{2+} sensitivity and force generation at 18 wk. Paralleling this loss of function is the change in the phosphorylation state of the contractile proteins in the TAC group. Such loss of function and change in protein phosphorylation was not seen at 18 wk in the AMI group, suggesting that HF caused by a pressure overload has a greater impact on the function of the diaphragm myofilaments and as a result requires greater compensation by the intact muscle to maintain function. While phosphorylation of cardiac myofilament proteins and the resultant effects on myofilament function are well described in both acute and chronic disease states, the role of such protein phosphorylation has been largely overlooked for skeletal muscle. Indeed, this work suggests, for the first time, that a decrease in the phosphorylation state of multiple myofilament proteins may be involved in initiating diaphragm dysfunction during the development of heart failure. Previously, loss of myosin content (66) and/or the increased levels of myosin heavy chain oxidation (8) have been described. While we did not observe any change in total myosin heavy chain content, given the progressive nature of the disease, our results do not preclude this from occurring at a later stage. Further, changes of the phosphorylation status of the myofilament and the resultant functional consequences could be independent of, or occur in conjunction with, alterations in the oxidative status. Clearly further work is needed to better understand the role of the myofilament in diaphragm dysfunction during the development of heart failure.

GRANTS

This work was supported by Discovery Grants from the Natural Sciences and Engineering Research Council of Canada (T. A. Gillis and J. A. Simpson) as well as equipment grants from the Canadian Foundation of Innovation (T. E. Gillis and J. A. Simpson). J. A. Simpson is a New Investigator of the Heart and Stroke Foundation of Canada.

DISCLOSURES

No conflicts of interest, financial or otherwise, are declared by the author(s).

AUTHOR CONTRIBUTIONS

Author contributions: T.E.G. and J.A.S. conception and design of research; T.E.G., J.M.K., A.J.F., M.J.P., J.S.H., and M.Y.C. performed experiments; T.E.G., J.M.K., A.J.F., M.J.P., J.S.H., and J.A.S. analyzed data; T.E.G., J.M.K., A.J.F., M.J.P., and J.A.S. interpreted results of experiments; T.E.G., J.M.K., A.J.F., M.Y.C., and J.A.S. prepared figures; T.E.G., J.M.K., and J.A.S. drafted manuscript; T.E.G. and J.A.S. edited and revised manuscript; T.E.G., J.M.K., A.J.F., M.J.P., J.S.H., M.Y.C., and J.A.S. approved final version of manuscript.

REFERENCES

1. **Adhikari BB, Regnier M, Rivera AJ, Kreutziger KL, Martyn DA.** Cardiac length dependence of force and force redevelopment kinetics with altered cross-bridge cycling. *Biophys J* 87: 1784–1794, 2004.
2. **Agbulut O, Noirez P, Beaumont F, Butler-Browne G.** Myosin heavy chain isoforms in postnatal muscle development of mice. *Biol Cell* 95: 399–406, 2003.
3. **Alderman SL, Klaiman JM, Deck CA, Gillis TE.** Effect of cold acclimation on troponin I isoform expression in striated muscle of rainbow trout. *Am J Physiol Regul Integr Comp Physiol* 303: R168–R176, 2012.
4. **Allwood MA, Kinobe RT, Ballantyne L, Romanova N, Melo LG, Ward CA, Brunt KR, Simpson JA.** Heme oxygenase-1 overexpression exacerbates heart failure with aging and pressure overload but is protective against isoproterenol-induced cardiomyopathy in mice. *Cardiovasc Pathol* 23: 231–237, 2014.
5. **Altringham JD, Young IS.** Power output and the frequency of oscillatory work in mammalian diaphragm muscle: the effects of animal size. *J Exp Biol* 157: 381–389, 1991.
6. **Brenner B.** Technique for stabilizing the striation pattern in maximally calcium-activated skinned rabbit psoas fibers. *Biophys J* 41: 99–102, 1983.

6a.(a)**Brenner B.** Effect of Ca^{2+} on cross-bridge turnover kinetics in skinned single rabbit psoas fibers: implications for regulation of muscle contraction. *Proc Natl Acad Sci USA* 85: 3265–3269, 1988.

6b.(b)**Brenner B, Eisenberg E.** Rate of force generation in muscle: correlation with actomyosin ATPase activity in solution. *Proc Natl Acad Sci USA* 83: 3542–3546, 1986.

6c.(c)**Chalovich JM, Chock PB, Eisenberg E.** Mechanism of action of troponin. tropomyosin. Inhibition of actomyosin ATPase activity without inhibition of myosin binding to actin. *J Biol Chem* 256: 575–578, 1981.

7. **Chemla D, Scalbert E, Desche P, Pourny JC, Lambert F, Lecarpentier Y.** Effects of perindopril on myocardial inotropy, lusitropy and economy, and on diaphragmatic contractility in the cardiomyopathic Syrian hamster. *J Pharmacol Exp Ther* 262: 516–525, 1992.
8. **Coirault C, Guellich A, Barbry T, Samuel JL, Riou B, Lecarpentier Y.** Oxidative stress of myosin contributes to skeletal muscle dysfunction in rats with chronic heart failure. *Am J Physiol Heart Circ Physiol* 292: H1009–H1017, 2007.
9. **Coirault C, Langeron O, Lambert F, Blanc FX, Lerebours G, Claude N, Riou B, Chemla D, Lecarpentier Y.** Impaired skeletal muscle performance in the early stage of cardiac pressure overload in rabbits: beneficial effects of angiotensin-converting enzyme inhibition. *J Pharmacol Exp Ther* 291: 70–75, 1999.
10. **De Sousa E, Veksler V, Bigard X, Mateo P, Serrurier B, Ventura-Clapier R.** Dual influence of disease and increased load on diaphragm muscle in heart failure. *J Mol Cell Cardiol* 33: 699–710, 2001.
11. **De Troyer A, Estenne M, Yernault JC.** Disturbance of respiratory muscle function in patients with mitral valve disease. *Am J Med* 69: 867–873, 1980.
12. **Drexler H, Riede U, Munzel T, Konig H, Funke E, Just H.** Alterations of skeletal muscle in chronic heart failure. *Circulation* 85: 1751–1759, 1992.
13. **Farah CS, Miyamoto CA, Ramos CH, da Silva AC, Quaggio RB, Fujimori K, Smillie LB, Reinach FC.** Structural and regulatory functions of the NH2- and COOH-terminal. *J Biol Chem* 269: 5230–5240, 1994.

14. **Ferreira LF, Moylan JS, Stasko S, Smith JD, Campbell KS, Reid MB.** Sphingomyelinase depresses force and calcium sensitivity of the contractile apparatus in mouse diaphragm muscle fibers. *J Appl Physiol (1985)* 112: 1538–1545, 2012.
15. **Funk M, Krumholz HM.** Epidemiologic and economic impact of advanced heart failure. *J Cardiovasc Nursing* 10: 1–10, 1996.
16. **Gillis TE, Klaiman JM.** The influence of PKA treatment on the Ca^{2+} activation of force generation by trout cardiac muscle. *J Exp Biol* 214: 1989–1996, 2011.
17. **Gillis TE, Liang B, Chung F, Tibbits GF.** Increasing mammalian cardiomyocyte contractility with residues identified in trout troponin C. *Physiol Genomics* 22: 1–7, 2005.
18. **Gillis TE, Martyn DA, Rivera AJ, Regnier M.** Investigation of thin filament near-neighbour regulatory unit interactions during force development in skinned cardiac and skeletal muscle. *J Physiol* 580: 561–576, 2007.
19. **Gordon AM, Homsher E, Regnier M.** Regulation of contraction in striated muscle. *Physiol Rev* 80: 853–924, 2000.
20. **Grange RW, Vandenboom R, Houston ME.** Physiological significance of myosin phosphorylation in skeletal muscle. *Can J Appl Physiol* 18: 229–242, 1993.
21. **Hammond MD, Bauer KA, Sharp JT, Rocha RD.** Respiratory muscle strength in congestive heart failure. *Chest* 98: 1091–1094, 1990.
22. **Harrison SM, Bers DM.** Modification of temperature dependence of myofilament Ca sensitivity by troponin C replacement. *Am J Physiol Cell Physiol* 258: C282–C288, 1990.
23. **Hart N, Kearney MT, Pride NB, Green M, Lofaso F, Shah AM, Moxham J, Polkey MI.** Inspiratory muscle load and capacity in chronic heart failure. *Thorax* 59: 477–482, 2004.
24. **Howell S, Maarek JM, Fournier M, Sullivan K, Zhan WZ, Sieck GC.** Congestive heart failure: differential adaptation of the diaphragm and latissimus dorsi. *J Appl Physiol* 79: 389–397, 1995.
25. **Jaber S, Petrof BJ, Jung B, Chanques G, Berthet JP, Rabuel C, Bouyabrine H, Courouble P, Koechlin-Ramonatxo C, Sebbane M, Similowski T, Scheuermann V, Mebazaa A, Capdevila X, Mornet D, Mercier J, Lacampagne A, Philips A, Matecki S.** Rapidly progressive diaphragmatic weakness and injury during mechanical ventilation in humans. *Am J Respir Crit Care Med* 183: 364–371, 2011.
26. **Keller A, Nesvizhskii AI, Kolker E, Aebersold R.** Empirical statistical model to estimate the accuracy of peptide identifications made by MS/MS and database search. *Anal Chem* 74: 5383–5392, 2002.
27. **Layland J, Solaro RJ, Shah AM.** Regulation of cardiac contractile function by troponin I phosphorylation. *Cardiovasc Res* 66: 12–21, 2005.
28. **Lecarpentier Y, Coirault C, Langeron O, Blanc FX, Salmeron S, Attal P, Riou B, Chemla D.** Impaired load dependence of diaphragm relaxation during congestive heart failure in the rabbit. *J Appl Physiol* 87: 1339–1345, 1999.
29. **Levine S, Nguyen T, Taylor N, Friscia ME, Budak MT, Rothenberg P, Zhu J, Sachdeva R, Sonnad S, Kaiser LR, Rubinstein NA, Powers SK, Shrager JB.** Rapid disuse atrophy of diaphragm fibers in mechanically ventilated humans. *N Engl J Med* 358: 1327–1335, 2008.
30. **Lindsay DC, Lovegrove CA, Dunn MJ, Bennett JG, Pepper JR, Yacoub MH, Poole-Wilson PA.** Histological abnormalities of muscle from limb, thorax and diaphragm in chronic heart failure. *Eur Heart J* 17: 1239–1250, 1996.
31. **Lipkin DP, Jones DA, Round JM, Poole-Wilson PA.** Abnormalities of skeletal muscle in patients with chronic heart failure. *Int J Cardiol* 18: 187–195, 1988.
32. **Lu QW, Hinken AC, Patrick SE, Solaro RJ, Kobayashi T.** Phosphorylation of cardiac troponin I at protein kinase C site threonine 144 depresses cooperative activation of thin filaments. *J Biol Chem* 285: 11810–11817, 2010.
33. **Lunde PK, Dahlstedt AJ, Bruton JD, Lannergren J, Thoren P, Sejersted OM, Westerblad H.** Contraction and intracellular Ca^{2+} handling in isolated skeletal muscle of rats with congestive heart failure. *Circ Res* 88: 1299–1305, 2001.
34. **Mancini DM, Coyle E, Coggan A, Beltz J, Ferraro N, Montain S, Wilson JR.** Contribution of intrinsic skeletal muscle changes to ^{31}P NMR skeletal muscle metabolic abnormalities in patients with chronic heart failure. *Circulation* 80: 1338–1346, 1989.
35. **Mancini DM, Henson D, LaManca J, Levine S.** Respiratory muscle function and dyspnea in patients with chronic congestive heart failure. *Circulation* 86: 909–918, 1992.
36. **McParland C, Krishnan B, Wang Y, Gallagher CG.** Inspiratory muscle weakness and dyspnea in chronic heart failure. *Am Rev Respir Dis* 146: 467–472, 1992.
37. **Meder B, Laufer C, Hassel D, Just S, Marquart S, Vogel B, Hess A, Fishman MC, Katus HA, Rottbauer W.** A single serine in the carboxyl terminus of cardiac essential myosin light chain-1 controls cardiomyocyte contractility in vivo. *Circ Res* 104: 650–659, 2009.
38. **Moreno-Gonzalez A, Gillis TE, Rivera AJ, Chase PB, Martyn DA, Regnier M.** Thin-filament regulation of force redevelopment kinetics in rabbit skeletal muscle fibres. *J Physiol* 579: 313–326, 2007.
39. **Nelson WB, Smuder AJ, Hudson MB, Talbert EE, Powers SK.** Cross-talk between the calpain and caspase-3 proteolytic systems in the diaphragm during prolonged mechanical ventilation. *Crit Care Med* 40: 1857–1863, 2012.
40. **Nesvizhskii AI, Keller A, Kolker E, Aebersold R.** A statistical model for identifying proteins by tandem mass spectrometry. *Anal Chem* 75: 4646–4658, 2003.
41. **Noland TA Jr, Guo X, Raynor RL, Jideama NM, Averyhart-Fullard V, Solaro RJ, Kuo JF.** Cardiac troponin I mutants Phosphorylation by protein kinases C and A and regulation of Ca^{2+}-stimulated MgATPase of reconstituted actomyosin S-1. *J Biol Chem* 270: 25445–25454, 1995.
42. **Persechini A, Stull JT, Cooke R.** The effect of myosin phosphorylation on the contractile properties of skinned rabbit skeletal muscle fibers. *J Biol Chem* 260: 7951–7954, 1985.
43. **Powers SK, Wiggs MP, Sollanek KJ, Smuder AJ.** Ventilator-induced diaphragm dysfunction: cause and effect. *Am J Physiol Regul Integr Comp Physiol* 305: R464–R477, 2013.
44. **Ribeiro PA, Ribeiro JP, Minozzo FC, Pavlov I, Leu NA, Kurosaka S, Kashina A, Rassier DE.** Contractility of myofibrils from the heart and diaphragm muscles measured with atomic force cantilevers: Effects of heart-specific deletion of arginyl-tRNA-protein transferase. *Int J Cardiol* 168: 3564–3571, 2013.
45. **Roberts BM, Ahn B, Smuder AJ, Al-Rajhi M, Gill LC, Beharry AW, Powers SK, Fuller DD, Ferreira LF, Judge AR.** Diaphragm and ventilatory dysfunction during cancer cachexia. *FASEB J* 27: 2600–2610, 2013.
46. **Roger VL, Go AS, Lloyd-Jones DM, Adams RJ, Berry JD, Brown TM, Carnethon MR, Dai S, de Simone G, Ford ES, Fox CS, Fullerton HJ, Gillespie C, Greenlund KJ, Hailpern SM, Heit JA, Ho PM, Howard VJ, Kissela BM, Kittner SJ, Lackland DT, Lichtman JH, Lisabeth LD, Makuc DM, Marcus GM, Marelli A, Matchar DB, McDermott MM, Meigs JB, Moy CS, Mozaffarian D, Mussolino ME, Nichol G, Paynter NP, Rosamond WD, Sorlie PD, Stafford RS, Turan TN, Turner MB, Wong ND, Wylie-Rosett J; American Heart Association Statistics Committee, and Stroke Statistics Subcommittee.** Heart disease and stroke statistics–2011 update: a report from the American Heart Association. *Circulation* 123: e18–e209, 2011.
47. **Sassoon CS, Caiozzo VJ, Manka A, Sieck GC.** Altered diaphragm contractile properties with controlled mechanical ventilation. *J Appl Physiol (1985)* 92: 2585–2595, 2002.
48. **Shanely RA, Van Gammeren D, Deruisseau KC, Zergeroglu AM, McKenzie MJ, Yarasheski KE, Powers SK.** Mechanical ventilation depresses protein synthesis in the rat diaphragm. *Am J Respir Crit Care Med* 170: 994–999, 2004.
49. **Simpson JA, Iscoe S.** Cardiorespiratory failure in rat induced by severe inspiratory resistive loading. *J Appl Physiol* 102: 1556–1564, 2007.
50. **Simpson JA, Labugger R, Collier C, Brison RJ, Iscoe S, Van Eyk JE.** Fast and slow skeletal troponin I in serum from patients with various skeletal muscle disorders: a pilot study. *Clin Chem* 51: 966–972, 2005.
51. **Simpson JA, van Eyk JE, Iscoe S.** Hypoxemia-induced modification of troponin I and T in canine diaphragm. *J Appl Physiol* 88: 753–760, 2000.
52. **Solaro RJ, Moir AJ, Perry SV.** Phosphorylation of troponin I and the inotropic effect of adrenaline in the perfused rabbit heart. *Nature* 262: 615–617, 1976.
53. **Stassijns G, Gayan-Ramirez G, De Leyn P, Verhoeven G, Herijgers P, de Bock V, Dom R, Lysens R, Decramer M.** Systolic ventricular dysfunction causes selective diaphragm atrophy in rats. *Am J Respir Crit Care Med* 158: 1963–1967, 1998.
54. **Stull JT, Kamm KE, Vandenboom R.** Myosin light chain kinase and the role of myosin light chain phosphorylation in skeletal muscle. *Arch Biochem Biophys* 510: 120–128, 2011.
55. **Sullivan MJ, Duscha BD, Klitgaard H, Kraus WE, Cobb FR, Saltin B.** Altered expression of myosin heavy chain in human skeletal muscle in chronic heart failure. *Med Sci Sports Exerc* 29: 860–866, 1997.

56. **Sullivan MJ, Green HJ, Cobb FR.** Skeletal muscle biochemistry and histology in ambulatory patients with long-term heart failure. *Circulation* 81: 518–527, 1990.
57. **Sumandea MP, Pyle WG, Kobayashi T, de Tombe PP, Solaro RJ.** Identification of a functionally critical protein kinase C phosphorylation residue of cardiac troponin T. *J Biol Chem* 278: 35135–35144, 2003.
58. **Supinski G, DiMarco A, Dibner-Dunlap M.** Alterations in diaphragm strength and fatiguability in congestive heart failure. *J Appl Physiol* 76: 2707–2713, 1994.
59. **Sweeney HL, Bowman BF, Stull JT.** Myosin light chain phosphorylation in vertebrate striated muscle: regulation and function. *Am J Physiol Cell Physiol* 264: C1085–C1095, 1993.
60. **Sweeney HL, Stull JT.** Alteration of cross-bridge kinetics by myosin light chain phosphorylation in rabbit skeletal muscle: implications for regulation of actin-myosin interaction. *Proc Natl Acad Sci USA* 87: 414–418, 1990.
61. **Tallis J, James RS, Little AG, Cox VM, Duncan MJ, Seebacher F.** Early effects of ageing on the mechanical performance of isolated locomotory (EDL) and respiratory (diaphragm) skeletal muscle using the work-loop technique. *Am J Physiol Regul Integr Comp Physiol* 307: R670–R684, 2014.
62. **Testelmans D, Crul T, Maes K, Agten A, Crombach M, Decramer M, Gayan-Ramirez G.** Atrophy and hypertrophy signalling in the diaphragm of patients with COPD. *Eur Respir J* 35: 549–556, 2010.
63. **Tikunov B, Levine S, Mancini D.** Chronic congestive heart failure elicits adaptations of endurance exercise in diaphragmatic muscle. *Circulation* 95: 910–916, 1997.
64. **Tikunov BA, Mancini D, Levine S.** Changes in myofibrillar protein composition of human diaphragm elicited by congestive heart failure. *J Mol Cell Cardiol* 28: 2537–2541, 1996.
65. **Van Eyk JE, Powers F, Law W, Larue C, Hodges RS, Solaro RJ.** Breakdown and release of myofilament proteins during ischemia and ischemia/reperfusion in rat hearts: identification of degradation products and effects on the pCa-force relation. *Circ Res* 82: 261–271, 1998.
66. **van Hees HW, van der Heijden HF, Ottenheijm CA, Heunks LM, Pigmans CJ, Verheugt FW, Brouwer RM, Dekhuijzen PN.** Diaphragm single-fiber weakness and loss of myosin in congestive heart failure rats. *Am J Physiol Heart Circ Physiol* 293: H819–H828, 2007.
67. **Westfall MV, Rust EM, Metzger JM.** Slow skeletal troponin I gene transfer, expression, and myofilament incorporation enhances adult cardiac myocyte contractile function. *Proc Natl Acad Sci USA* 94: 5444–5449, 1997.